Journal of Applied Electrochemistry **31**: 1–11, 2001.
© 2001 *Kluwer Academic Publishers. Printed in the Netherlands.*

Modelling electrochemical impedance data for semi-bipolar lead acid batteries

H. ANDERSSON[1]*, I. PETERSSON[2] and E. AHLBERG[2]
[1]*Department of Environmental Inorganic Chemistry, Chalmers University of Technology, S-412 96, Göteborg Sweden*
[2]*Department of Chemistry, Göteborg University, S-412 96, Göteborg Sweden*
*(*author for correspondence)*

Received 15 October 1999; accepted in revised form 19 July 2000

Key words: electrochemical impedance spectroscopy, lead–acid batteries, lead dioxide, porous electrodes

Abstract

Electrochemical impedance spectroscopy offers an alternative method of performing nondestructive characterisation of electrodes and batteries in stationary power stations compared to the more conventional discharge tests. A model for porous electrodes is used to analyse impedance data in such a way that physical parameters can be evaluated. It is also suggested that these parameters can be used as a way of determining the state of health of a battery during float charging. A method for the calculation of the steady-state current of porous electrodes is also presented, based on the impedance model. The combined d.c. and a.c. analysis confirm more concisely the validity of the theoretical assumptions used to explain the experimental data.

List of symbols

A	geometric area of the electrode (cm^2)
C_{dl}	double layer capacitance per active surface unit ($F\,cm^{-2}$)
C_{tot}	total electrode capacitance ($F\,cm^{-2}$)
β	a frequency-dependent impedance parameter (cm^{-1})
β_{max}	maximum surface concentration of θ (mol cm^{-2})
d	thickness of the electrode (cm)
f	tortuosity factor (dimensionless)
i_f	faradaic current of a planar electrode (A cm^{-2})
i_{por}	faradaic current of a porous electrode (A cm^{-2})
K	field diffusion constant ($cm^2\,s^{-1}$)
R	gas constant (J mol^{-1} K^{-1})
R_{ct}	charge transfer resistance ($\Omega\,cm^2$)
R_p	steady-state polarization resistance for a planar electrode ($\Omega\,cm^2$)
R_0	steady-state polarization resistance for a porous electrode ($\Omega\,cm^2$)
R_{por}	pore resistance (Ω)
S_c	active surface area per volume (cm^{-1})
v_p	relative pore volume (dimensionless)
l_p	characteristic pore dimension (cm)
$Z(\omega)$	interfacial porous impedance (Ω)
Z_f	faradaic impedance of a planar electrode ($\Omega\,cm^2$)
τ	time constant (s)
ρ_1	resistivity of the electrode (Ω cm)
ρ_2	effective resistivity of the electrolyte in the porous electrode (Ω cm)
ρ_2^*	resistivity of the bulk electrolyte (Ω cm)
ω_0	frequency related to the rate of the reaction (s^{-1})
ω_1	frequency related to field diffusion and thickness of porous electrode (s^{-1})
ω_{max}	frequency at maximum of imaginary part of impedance (s^{-1})
$\vec{k_i}$	forward potential dependent rate constant for reaction i (mol cm^{-2} s^{-1})
$\overleftarrow{k_i}$	backward potential dependent rate constant for reaction i (mol cm^{-2} s^{-1})
k_i°	rate constant for reaction i at E° (mol cm^{-2} s^{-1})
α_i	transfer coefficient (dimensionless)
$\vec{b_i}$	Tafel coefficient for the forward reaction i (V^{-1})
$\overleftarrow{b_i}$	Tafel coefficient for the backward reaction i (V^{-1})
b_{pl}	Tafel slope for a planar electrode (V)
b_{por}	Tafel slope for a porous electrode (V)
E	electrode potential (V)
E°	reference electrode potential (V)
η	surface factor (dimensionless)
ς	resistance ($\Omega\,cm^2$)
λ	rate factor (dimensionless)
Φ	work function

1. Introduction

Electrochemical impedance spectroscopy (EIS) has been suggested as a technique for measuring the state of charge or state of health of batteries [1]. In stationary power stations of today the most common technique is to perform complete discharge tests. This is time consuming and expensive and it also requires the

disconnection of the battery cells from the operational circuit. EIS may provide an attractive nondestructive alternative to discharge tests. Viswanathan et al. [2, 3] determined the state of charge of commercial sealed Ni–Cd and lead acid cells by using a modified Randles equivalent circuit in the data analysis. It was claimed that the ohmic resistance decreased, while the charge transfer resistance and the nonideal double layer capacitance increased with an increase in the state of charge. In particular, they found their data sensitive to the state-of-charge at low frequencies (0.06–0.9 Hz). Similarly, Barton et al. [4] found that the ohmic resistance decreases with increasing state-of-charge. Since this result is consistent with the specific gravity of the electrolyte they used the ohmic resistance as a characteristic parameter for prediction of the state-of-charge of maintenance-free lead–acid batteries. The frequency corresponding to the maximum on the high frequency semicircle of the Nyquist diagram was used by Hughes et al. [5] to calculate the characteristic product of charge transfer resistance and double layer capacitance for prediction of the state-of-charge of a sealed lead–acid battery. Jindra et al. [6] measured the impedance of both sealed lead–acid batteries and of the two electrodes separately during galvanostatic charging. At 0.1 Hz the impedance increased dramatically, due to the increase in internal pressure during overcharging. The increase in the impedance curve was used to indicate the fully charged cell.

For a physical model of the impedance characteristics of battery systems a porous matrix has to be treated. The basic theory for porous electrodes was formulated by de Levie [7, 8] who derived analytical solutions for the a.c. impedance assuming cylindrical pores with constant radius, semiinfinite length and no concentration gradients along the pore axis. Using numerical methods it was possible to consider different pore geometries of the electrode [9, 10] and diffusion of reactants along the centre of the pore axis [11]. A more general treatment regarding the pore geometry was presented by Paasch et al. [12] by considering the electrode to be macrohomogeneous. The model is somewhat simplified with respect to the diffusion, which is assumed to be planar.

The relationship between impedance and pore geometry has been used to determine the radius, pore length and number of pores for gold-powder and Raney-gold electrodes [13]. Further, the pore texture of Raney-nickel electrodes in the liquid-phase has been determined by impedance, with good correlation to the surface area as measured using established gas phase techniques [14]. The cylindrical pore model has also been used to predict the pore texture of packed zinc particles of irregular shape in both a noncorrosive electrolyte [15], and in a corrosive acidic electrolyte [16].

In an earlier study [17] EIS was used to study changes in resistance and porosity for Planté formed, porous lead dioxide electrodes in 5 M H_2SO_4. Lead dioxide electrodes made from 100, 200 and 400 μm lead foils were investigated with and without an external mechanical pressure in a wide potential region, ranging from 0.5 to 1.5 V. At these different potentials, impedance spectra were taken as a function of the thickness of the preformed oxide layer and of the mechanical pressure exerted on the cells. The results showed that the total IR-drop was due to contributions from porosity, electrolyte resistance and lack of interparticle contact. The contributions from the porosity and the bulk electrolyte resistances were found to be small compared to the contribution from the interparticle contact (i.e., the lack of interparticle contact) to the total IR-loss. The best interparticle contact was found for the least porous material. As a complement to the impedance study, specific area and pore volume measurements of the three different electrode thicknesses used in the study were made in order to gain more information about the texture of the porous lead dioxide electrode [17]. In the present study an impedance model for porous electrodes [12] was used to analyse the impedance data from the former study [17]. The impedance analysis was focused on potentials corresponding to float charge (1.3–1.5 V vs Hg/Hg_2SO_4) and enabled the evaluation of physical parameters such as polarization resistance, double layer capacitance, relative pore volume, specific surface area and/or effective resistance. These parameters can be used in a diagnostic way to determine the state of health of the battery during float charging.

2. Porous electrodes

2.1. *The model*

The model [12] considers a charge transfer process taking place at the interface of a conducting macrohomogeneous porous electrode with a geometric area, A and thickness, d. The electrode is perturbed by a small a.c. signal and subjected to appropriate boundary conditions. That is, Ohm's law holds for electrons and ions at the contact side and electrolyte side of the electrode, respectively. Charge transport is carried out by electrons in the electrode and ions in the electrolyte. Averaging the resulting time and position dependent potential over the volume element $A\,\mathrm{d}x$, containing many pores with a characteristic dimension $l_p \ll d$, and assuming constant concentrations of electroactive compounds it is possible to derive the following impedance function (Equation 22 in reference 12):

$$AZ(\omega) = \frac{\rho_1^2 + \rho_2^2}{\rho_1 + \rho_2}\frac{1}{\beta}\coth(\beta \cdot d) + 2\frac{\rho_1\rho_2}{\rho_1 + \rho_2}\frac{1}{\beta\ \sinh(\beta \cdot d)} + d\frac{\rho_1\rho_2}{\rho_1 + \rho_2} \qquad (1)$$

If the resistivity of the electrode, ρ_1, is considerably lower than the resistivity of the electrolyte in the porous

electrode, ρ_2, the last two terms can be neglected and Equation 1 is reduced to

$$AZ(\omega) = \frac{\rho_2}{\beta}\coth(\beta \cdot d) \tag{2}$$

The frequency dependent parameter β can be written as

$$\beta = \sqrt{\frac{\omega_0 + j\omega}{K}} \tag{3}$$

where ω_0 is a frequency related to the kinetics of the reaction. For simple charge transfers $\omega_0 = 1/R_{ct}C_{dl}$. In general, one has to consider all the processes that determine the rate of the faradaic process. In that cases ω_0 should be replaced with $1/Z_fC_{dl}$, where Z_f is the frequency-dependent faradaic impedance. For ideally polarizable electrodes, where no charge transfer occurs, ω_0 is zero (e.g., double-layer capacitors). Parameter K depends on the double-layer capacity and the ohmic resistivity in the solution. It can be regarded as a diffusion constant for the propagation of the electric field in the electrolyte distributed in the pores of the electrode. Defining a field diffusion frequency,

$$\omega_1 = \frac{K}{d^2} \tag{4}$$

where

$$K = \frac{1}{C_{dl}S_c\rho_2} \quad (\rho_2 \gg \rho_1) \tag{5}$$

the electrochemical impedance of a charge transfer limited reaction at a macrohomogeneous porous electrode is determined by the parameters, ρ_2, d, ω_0 and ω_1.

$$AZ(\omega) = \rho_2 d\sqrt{\frac{\omega_1}{\omega_0 + j\omega}}\coth\left(\sqrt{\frac{\omega_0 + j\omega}{\omega_1}}\right) \tag{6}$$

The resistivity of the electrolyte in the pores, ρ_2, is related to the bulk electrolyte resistivity, ρ_2^*, and the relative pore volume, v_p, in the following way:

$$\rho_2 = \frac{\rho_2^* f}{v_p} \tag{7}$$

where f is the tortuosity factor.

2.2. *Impedance characteristics of the model*

At high frequencies, the impedance shows a transmission line behaviour (i.e., a 45° slope in the complex impedance plane. At lower frequencies, two extreme cases can be distinguished depending on the ratio between ω_1 and ω_0. First, when $\omega_1 \gg \omega_0$, the impedance corresponds to a slow electron transfer reaction or a thin electrode. Noting that $\coth(x) \to 1/x$ when $x \to 0$, Equation 6 can be approximated with

$$AZ(\omega) = \rho_2 d\frac{\omega_1}{\omega_0 + j\omega} \tag{8}$$

which traces a semicircle in the complex impedance plane with a diameter of $R_0 = \rho_2 d\omega_1/\omega_0$ and a maximum of the imaginary part, ω_{max}, at ω_0, Figure 1(a). Thus, R_0 is the impedance at zero frequency. Secondly, when $\omega_1 \ll \omega_0$, the impedance corresponds to a fast electron transfer reaction or a thick electrode. Since $\coth x \to 1$ when $x \to \infty$, Equation (6) can be approximated with

$$AZ(\omega) = \rho_2 d\sqrt{\frac{\omega_1}{\omega_0 + j\omega}} \tag{9}$$

which traces a skewed arc in the complex impedance plane with a zero frequency end at $R_0 = \rho_2 d\sqrt{\omega_1/\omega_0}$ and a maximum of the imaginary part, ω_{max}, at $\sqrt{3}\omega_0$, Figure 1(b). For nonextreme cases and when there is a clear distinction between a transmission line part of the

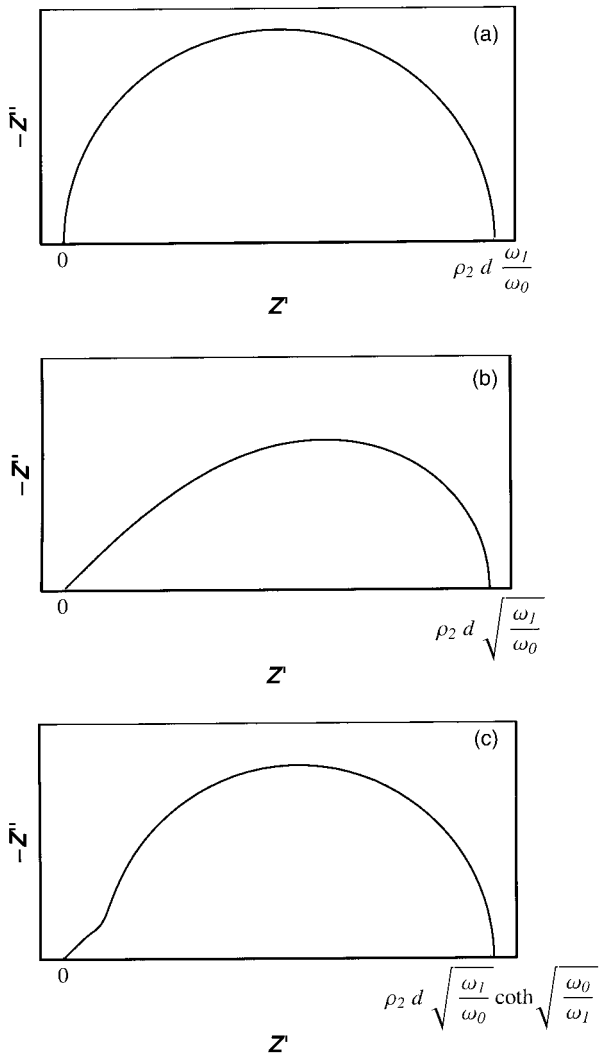

Fig. 1. Schematic representation of three characteristic impedance diagrams generated by the porous model: (a) $\omega_1 \gg \omega_0$, corresponding to a slow electron transfer reaction or a thin electrode, (b) $\omega_1 \ll \omega_0$, simulating a fast charge transfer reaction or thick electrode, and (c) the intermediate case.

spectrum at high frequencies and a well developed semicircle in the rest of the spectrum, the following approximation (Equation 10) can be used for estimation of ω_1.The linear high frequency part of the spectrum will in this case change into a semicircle like arc at a point where the real part of the impedance is close to $R_{por} = \rho_2 d/3$ [10]. The impedance at zero frequency, R_0, may in this case be approximated to $R_0 = \rho_2 d(1/3 + \omega_1/\omega_0)$, Figure 1(c). The following relation can then be derived which gives ω_1 as

$$\omega_1 \approx \frac{\omega_0}{3}\left(\frac{R_0}{R_{por}} - 1\right) \tag{10}$$

where ω_0 is close to the maximum frequency, ω_{max}. To verify that ω_0 can be approximated by ω_{max} in the intermediate range, ω_{max} was calculated numerically as a function of $\log(\omega_1/\omega_0)$. It was found that the approximation is valid to within 1% relative error as long as the ratio ω_1/ω_0 is greater than 1.58.

Using the result from [12] and assuming a kinetically controlled charge transfer process with the charge transfer resistance, R_{ct}, the following relations can be formulated:

$$\omega_0 = \frac{1}{R_{ct}C_{dl}} \tag{11}$$

$$\omega_1 = \frac{1}{d^2 C_{dl} S_c \rho_2} \tag{12}$$

If the process of interest involves more complex kinetics, ω_0 has to be replaced by $1/Z_f C_{dl}$, where Z_f is the faradaic impedance of a planar electrode. Diffusion and intercalation kinetics in connection to porous electrodes have for example been treated in [12]. In this work a surface relaxation of $PbO_2/PbSO_4$ will be considered.

Irrespective of the kinetics, the impedance model for porous electrodes permits the use of ordinary planar electrode kinetics for the faradaic process. This is simply performed by substitution of ω_0 by $1/Z_f C_{dl}$ followed by insertion into Equations 6, 8 and 9, giving Equations 13–15.

For thin electrodes or slow charge reactions, the general impedance of a porous electrode is written as

$$AZ(\omega) = \frac{\eta Z_f}{1 + j\omega Z_f C_{dl}} \tag{13}$$

where $\eta = 1/(dS_c)$, can be regarded as a surface factor relating the true electrochemically active surface to the apparent macroscopic electrode area. For the other extreme case, fast reactions or thick electrodes, the impedance turns out to be

$$AZ(\omega) = \sqrt{\frac{\varsigma Z_f}{1 + j\omega Z_f C_{dl}}} \tag{14}$$

where $\varsigma = \rho_2/S_c$ is the apparent electrolyte resistance in the pores. In the intermediate range Equation 6 has to be used resulting in

$$AZ(\omega) = \rho_2 d\sqrt{\frac{\omega_1 Z_f C_{dl}}{1 + j\omega Z_f C_{dl}}}\coth\sqrt{\frac{1 + j\omega Z_f C_{dl}}{\omega_1 Z_f C_{dl}}} \tag{15}$$

To make use of Equations 13–15 the faradaic impedance, Z_f, must be known. In Section 4.2 the derivation of the faradaic impedance is outlined for the reactions considered in this paper.

2.3. *Derivation of the steady state current of a porous electrode from the impedance model*

The linear relation between $Z(\omega)$ and Z_f when $\omega \to 0$ in Equation 13 suggests that the steady state kinetics, that is, $\omega \to 0$ and $Z_f \to R_p$, for slow electrochemical reactions in porous electrodes obeys the same potential dependence as for planar electrodes. Thus, the Tafel slopes for porous electrodes will be the same as for planar electrodes. However, this is not true for fast reactions as indicated by the square root dependence between $Z(\omega)$ and Z_f when $\omega \to 0$ in Equation 14.

The potential dependent Tafel slope, b_{pl}, can for planar electrodes be written as

$$b_{pl} = \ln 10\, R_p i_f \tag{16}$$

and similarly for porous electrodes

$$b_{por} = \ln 10\, R_0 i_{por} \tag{17}$$

i_f is the faradaic steady-state current derived for planar electrodes using Butler–Volmer kinetics and R_p is the corresponding polarization resistance. i_{por} is the steady-state current of the porous electrode and R_0 is the polarization resistance, corresponding to the zero frequency resistance obtained from the impedance model of the porous electrode, Equations 13–15 with $\omega = 0$ and Z_f replaced by R_p. It is obvious that the ratio between the planar Tafel coefficient, b_{pl}, and its porous analogue, b_{por}, will change when the kinetics become fast since we have a linear relation between R_0 and R_p for slow reactions and a square root dependence for fast reactions, under steady state conditions. This shows that the apparent Tafel slope for porous electrodes is doubled at high reaction rates, in agreement with earlier findings [18]. Thus, we can calculate the faradaic current through a porous electrode from a planar model under extreme conditions (fast or slow faradaic reactions) using Equations 10 and 11 together with Equations 13 and 14. For intermediate conditions the following approach has been used. The relation $b_{por} = pb_{pl}$ is assigned, where p lies in the interval from 1 to 2 and depends on the ratio ω_0/ω_1. p is determined by a normalized impedance function Φ for a porous electrode at zero frequency (Equation 6), defined as

$$\Phi(\lambda) = \sqrt{10^{\lambda}} \coth \sqrt{10^{-\lambda}} \tag{18}$$

where $\lambda = \log[\omega_1/\omega_0]$. The function, Φ, mimics the impedance behaviour at steady state as a function of the logarithmic ratio between the two characteristic frequencies, ω_0 and ω_1. Derivation of $\log[\Phi\lambda)]$ followed by inversion gives the work function from which p can be determined from λ.

$$p(\lambda) = \frac{1}{\dfrac{\partial(\log[\Phi(\lambda)])}{\partial\lambda}} = \frac{2\coth\sqrt{10^{-\lambda}}}{\coth\sqrt{10^{-\lambda}} + \sqrt{10^{-\lambda}}\,\mathrm{cosech}\left(\sqrt{10^{-\lambda}}\right)^2} \tag{19}$$

A plot of $p(\lambda)$ in the λ-range corresponding to intermediate conditions is shown in Figure 2. p changes from 1 to 2 going from $\omega_0 \ll \omega_1(\lambda > 2)$ to $\omega_0 \gg \omega_1(\lambda < -2)$, that is a doubling of the Tafel slope proceeding from slow to fast reaction kinetics. Thus, the faradaic steady-state current in the porous electrode, i_{por} can be calculated from the electrochemical quantities of the planar electrode, i_f, R_p and C_{dl} given the physical properties of the porous electrode as expressed in ω_1 (Equation 12).

$$I_{por} = p(\lambda) I_f \frac{R_p}{R_0} \tag{20}$$

3. Experimental details

3.1. *Preparation of the lead dioxide electrodes*

The lead dioxide electrodes were prepared from pure lead foils (99.95%, Goodfellow) according to the Planté formation process described in detail by Petersson et al. [19].

Immediately prior to an experiment the lead foil was washed in 8 M HNO_3 (p.a., Merck) and rinsed in deionized milli-Q water. This was done to remove air formed oxides from the surface of the foil before it was immersed in the electrolyte solution for the start of the Planté formation process. The lead foils were pretreated cathodically for about 30 min at 1.5 mA cm^{-2} in an electrolyte consisting of 0.5 M H_2SO_4 containing 0.05 M $KClO_4$. The electrodes were then oxidized and reduced galvanostatically in the same electrolyte at 10 mA cm^{-2} to a thickness corresponding to the oxidation of 200 μm Pb foil. After the reduction process the perchlorate ions were rinsed from the electrodes with deionized milli-Q water and finally the positive electrodes were completely oxidized to PbO_2 in 1 M H_2SO_4.

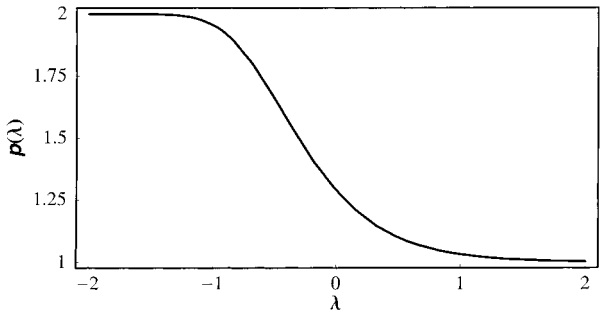

Fig. 2. $p(\lambda)$ as a function of the potential dependent parameter λ.

After the formation process the electrodes were assembled to 2 V laboratory cells, with the semibipolar electrodes used as working electrodes and a conventional pasted lead electrode (Tudor Nol, Sweden) as counter electrode, and stabilized by three charge–discharge cycles at 22 mA cm^{-2} in 5 M H_2SO_4. The equipment for the formation process consisted of a microprocessor controlled unit, a power supply and a multimeter, and was designed to send alternative anodic and cathodic currents through the cells. The time and the current density for each step in the process could be adjusted manually.

For the experiments shown in Figure 3, a lead rod with an area of 0.2 cm^2 was used. The electrode was cycled between 0.5 and 1.5 V 10 times before the impedance measurements were conducted. The electrode was held at the given potential 300 s before start of the measurement. The sweep rate was 20 mV s^{-1} and the electrode was stationary.

3.2. *Impedance measurements*

Electrochemical impedance measurements were performed at constant potential in the $PbSO_4/PbO_2$ region, 0.5 to 1.5 V. A frequency sweep from 100 kHz to 2 mHz was used with an amplitude of the applied sine wave of 5 mV r.m.s. Impedance spectra were taken of the preformed oxide layer and in the absence and presence of mechanical pressure. A 273A Princeton Applied Research (PAR) potentiostat/galvanostat and a Schlumberger frequency response analyzer SI1255 were used for the experiments. All potentials are referred to the $Hg/Hg_2SO_4/K_2SO_4$ reference electrode, E = 0.64 V vs NHE. 5 M H_2SO_4 (p.a., Merck) was used as electrolyte in all experiments. The current was measured during the acquiring of the spectra and was used to compensate the applied potential for the ohmic drop.

3.3. *Specific surface area*

The internal specific surface area (BET) was determined by measuring the low-temperature nitrogen adsorption using a FlowSorb II 2300 (Micromeritics). The lead dioxide powder was removed from the electrode and used directly without any further pretreatment.

3.4. *Porosity by water intrusion*

The relative pore volume, v_p, was measured by water intrusion. The parameter was obtained using

Archimedes' principle, where the difference in the weight of the sample in air compared to the weight suspended in water permits calculations of the volume. The sample was initially dry weight, A, and put under vacuum for at least 30 min. Then the sample was covered with distilled water still under vacuum and left to soak for 12 h. The wet weight of the sample was measured both in air, B, and suspended in water, C. From this information the exterior volume (B–C), the volume of the open pores (B–A) and apparent porosity (B–A/B–C) was calculated. The results were compensated for the underlying metal foil. The porosity was determined after the complete formation.

4. Results and discussion

In Figure 3 a cyclic voltammogram of a porous lead dioxide on a pure lead rod is shown, together with the characteristic impedance diagrams at the different potentials. The electrode was cycled 10 times in a wide region ranging from 0.5 to 1.5 V in the $PbSO_4/PbO_2$ region before the impedance measurements were performed. At 1 V (a), the charge transfer resistance is quite high due to the existence of an insulating $PbSO_4$ layer. When the potential is increased the formation of PbO_2 starts and the charge transfer resistance decreases, (b)–(d). At the most positive potentials the oxygen evolution reaction is the main contributor to the current and the impedance response shows fast electron transfer kinetics. This is illustrated in Figure 3(e) by the small diameter of the semicircle in the impedance diagram. On the back scan the charge transfer resistance increases again at less positive potentials (f)–(g). This is due to the formation of insulating $PbSO_4$. In this work, potentials corresponding to float charge of lead–acid batteries over 1.3–1.5 V, (c)–(e), will be considered.

4.1. *Steady-state reaction kinetics*

At the potentials of interest the oxygen evolution reaction occurs in parallel with the formation of lead dioxide from lead sulphate. By assuming that the oxygen evolution reaction only takes place on the conducting lead dioxide the reactions with corresponding rate equations can be formulated [20–22]:

$$PbSO_4 + 2\ H_2O \underset{\overleftarrow{k}_1}{\overset{\vec{k}_1}{\rightleftharpoons}} PbO_2 + 4\ H^+ + SO_4^{2-} + 2\ e^- \tag{21}$$

$$H_2O \xrightarrow{\vec{k}_2} \tfrac{1}{2}O_2 + 2\ H^+ + 2\ e^- \tag{22}$$

$$i_1 = 2\ F\left(\vec{k}_1(1-\theta) - \overleftarrow{k}_1\theta\right) \tag{23}$$

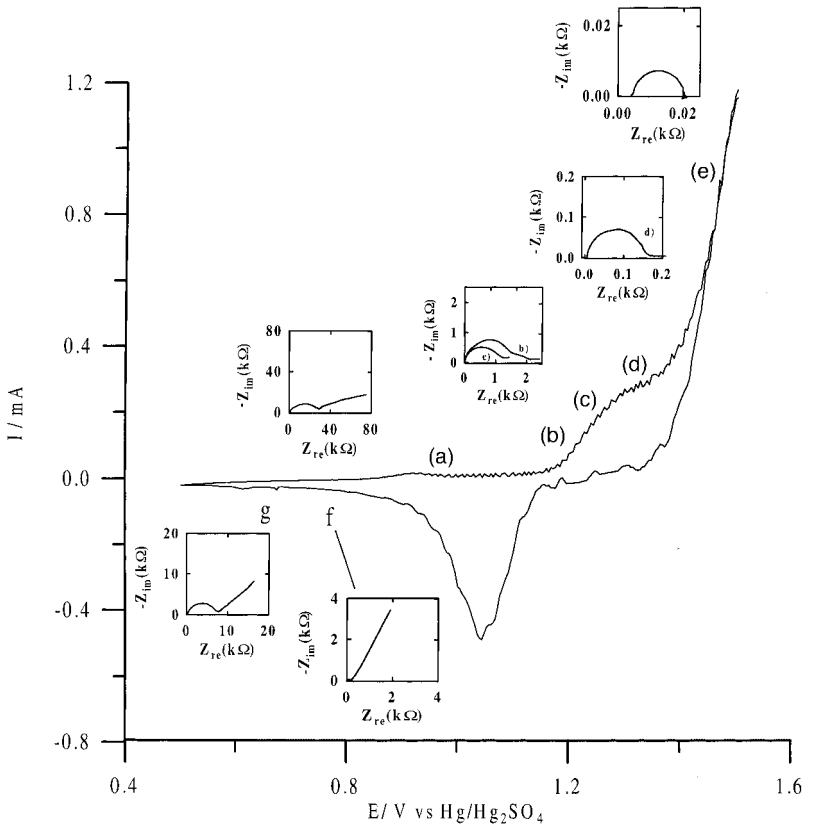

Fig. 3. A cyclic voltammogram of a stationary porous lead dioxide electrode cycled 10 times in 1 M H_2SO_4, together with the characteristic impedance diagrams at different potentials. (a) 0.95, (b) 1.2, (c) 1.3, (d) 1.4 and (e) 1.5 V on the positive going scan and (f) 0.75 and (g) 0.6 V on the negative going scan.

$$i_2 = 2F\vec{k_2}\,\theta \tag{24}$$

where θ is the electron conducting fraction of the electrode surface where the oxygen evolution reaction can take place. i_1 and i_2 are the current density of the PbO_2 formation and oxygen evolution, respectively, given as mA cm^{-2} of the geometric area of the electrode. F is the faradaic constant and $\vec{k_1}$ and $\vec{k_2}$ are the rate constants with the usual exponential potential dependence.

$$\vec{k}_{1,2} = k^0_{1,2}\exp\left(\frac{(1-\alpha_{1,2})2F\left(E - E^\circ_{1,2}\right)}{RT}\right) \tag{25a}$$

$$\overleftarrow{k}_1 = k^0_1\exp\left(\frac{-\alpha_1\,2F\left(E - E^\circ_1\right)}{RT}\right) \tag{25b}$$

The total current is thus simply the sum of the two contributions, $i_f = i_1 + i_2$. At the potentials of interest in this investigation, the second term in Equation 23 can be neglected.

Assuming a Langmuir isotherm, the steady-state solution of the conductive fraction of the electrode surface, θ_{ss}, is given by

$$\theta_{ss} = \frac{\vec{k}_1}{\vec{k}_1 + \overleftarrow{k}_1} \tag{26}$$

The faradaic steady-state current can thus be evaluated and is given by

$$i_f = 2F\left[\left(\frac{\vec{k}_1 - \vec{k}_1\overleftarrow{k}_1}{\vec{k}_1 + \overleftarrow{k}_1}\right) + \frac{\vec{k}_1\vec{k}_2}{\vec{k}_1 + \overleftarrow{k}_1}\right] \tag{27}$$

From this expression the polarization resistance can be derived

$$\frac{1}{R_p} = 2F\left(\vec{b}_1\vec{k}_1 + \frac{\left(\vec{b}_1 + \vec{b}_2\right)\vec{k}_1\vec{k}_2}{\vec{k}_1 + \overleftarrow{k}_1} - \frac{\left(\vec{b}_1\vec{k}_1 + \overleftarrow{b}_1\overleftarrow{k}_1\right)\left(\vec{k}_1\vec{k}_1 + \vec{k}_1\vec{k}_2\right)}{\left(\vec{k}_1 + \overleftarrow{k}_1\right)^2}\right) \tag{28}$$

4.2. *Transient reaction kinetics*

The impedance of the reactions considered in Section 4.1 is obtained by a first order Taylor expansion of the faradaic current response from a small sinusoidal voltage perturbation, $\Delta E = |\Delta E|\exp(j\omega t)$, where the amplitude of the perturbation, $|\Delta E|$, is less than 10 mV.

$$\Delta i_f = \left(\frac{\partial i_f}{\partial E}\right)_\theta \Delta E + \frac{\partial i_f}{\partial \theta}\Delta\theta \tag{29}$$

Dividing by ΔE gives the faradaic admittance, which is the reciprocal of the faradaic impedance, Z_f.

$$\frac{1}{Z_f} = \left(\frac{\partial i_f}{\partial E}\right)_\theta + \frac{\partial i_f}{\partial \theta}\frac{\Delta\theta}{\Delta E} \tag{30}$$

The right hand side of Equation 30 is obtained from the charge and mass balance relations derived from the reaction scheme (21 and 22).

$$i_f = 2F\left(\vec{k}_1(1-\theta) + \vec{k}_2\theta\right) \tag{31}$$

$$\beta_{max}\frac{d\theta}{dt} = \vec{k}_1(1-\theta) - \overleftarrow{k}_1\,\theta \tag{32}$$

where β_{max} is the maximum surface concentration of θ in mol cm^{-2}. This gives

$$\left(\frac{\partial i_f}{\partial E}\right)_\theta = \frac{1}{R_{ct}} = 2F\left(\vec{b}_1\vec{k}_1(1-\theta) + \vec{b}_2\vec{k}_2\theta\right) \tag{33}$$

$$\frac{\partial i_f}{\partial \theta} = 2F\left(\vec{k}_2 - \vec{k}_1\right) \tag{34}$$

$\Delta\theta$ is obtained by noting that its time variation can be written as

$$\frac{d\Delta\theta}{dt} = j\omega t\Delta\theta \tag{35}$$

Since θ is continuous and well behaved with respect to the potential, delta and the derivative operators can be switched. By taking the total differential of $d\theta/dt$ with respect to the potential and the potential dependent quantities, θ in this case, and using the steady-state values of θ, θ_{ss}, the following expression is obtained for $\Delta\theta/\Delta E$:

$$\frac{\Delta\theta}{\Delta E} = \frac{\vec{b}\vec{k}_1(1-\theta_{ss}) - \overleftarrow{b}_1\overleftarrow{k}_1\theta_{ss}}{-\vec{k}_1 - \overleftarrow{k}_1 + j\omega\beta_{max}} \tag{36}$$

Inserting Equations 33, 34 and 36 into Equation 30 gives the reciprocal faradaic impedance:

$$\frac{1}{Z_f} = 2F\left(\vec{b}_1\vec{k}_1\left(\vec{b}_2\vec{k}_2 - \vec{b}_1\vec{k}_1\right)\theta_{ss} - \left(\vec{k}_2 - \vec{k}_1\right) \times \frac{\left(\vec{b}_1\vec{k}_1(1-\theta_{ss}) - \overleftarrow{b}_1\overleftarrow{k}_1\theta_{ss}\right)\Big/\left(\vec{k}_1 + \overleftarrow{k}_1\right)}{1 + j\omega\tau}\right) \tag{37}$$

where $\tau = \beta_{max}/(\vec{k}_1 + \overleftarrow{k}_1)$ is the time constant for the relaxation of θ. The interfacial impedance for the porous electrode is then given by

$$AZ(\omega) = \rho_2 d\sqrt{\frac{\omega_1 Z_f C_{dl}}{1 + j\omega Z_f C_{dl}}}\coth\sqrt{\frac{1 + j\omega Z_f C_{dl}}{\omega_1 Z_f C_{dl}}} \tag{38}$$

4.3. *Interpretation of the experimental results*

Figure 4(a) shows the experimental steady-state currents measured during the acquiring of the impedance spectra

together with the calculated steady-state current, i_{por} (Equation 20), while the corresponding experimental and theoretical polarization resistances are given in Figure 4(b). The polarization resistance is calculated for $\omega = 0$, according to Equation 15. In Figure 5, similar data for the pressurized electrode are given. The parameter values used in the simulation are given in Table 1. The current for the pressurized electrode, Figure 5, is larger than for the nonpressurized electrode. This can be explained by the fact that the pressurized electrode has a lower interparticle resistance [17], which facilitates the oxygen evolution reaction.

The agreement between the experimental data and the model is good. However, for the nonpressurized electrode the experimentally obtained currents are lower than the model predicts. This can be explained by the porous nature of the electrode, which in the nonpressurized condition permits movement of the active material.

4.4. *Impedance behaviour*

Impedance measurements of Planté formed lead dioxide showed the characteristic features of a porous electrode, Figures 6 and 7. The Nyquist plots of all spectra on the lead electrodes were linear in the high frequency part with a slope between 35° and 45°. At 1.29 and 1.38 V the low frequency part of the spectra were characterised by a slightly depressed semicircle with a potential dependent diameter. The depression of the semicircle at 1.29 V is in fact reflected in the simulated spectra, where the surface

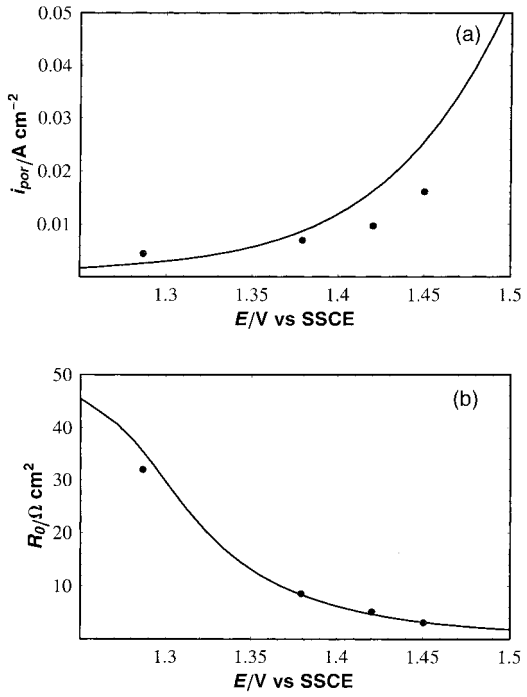

Fig. 4. Experimental values (•) for the steady-state current (a) and the zero frequency resistance (b) of the porous PbO_2-electrode plotted together with the theoretical curve (solid line). Without external pressure.

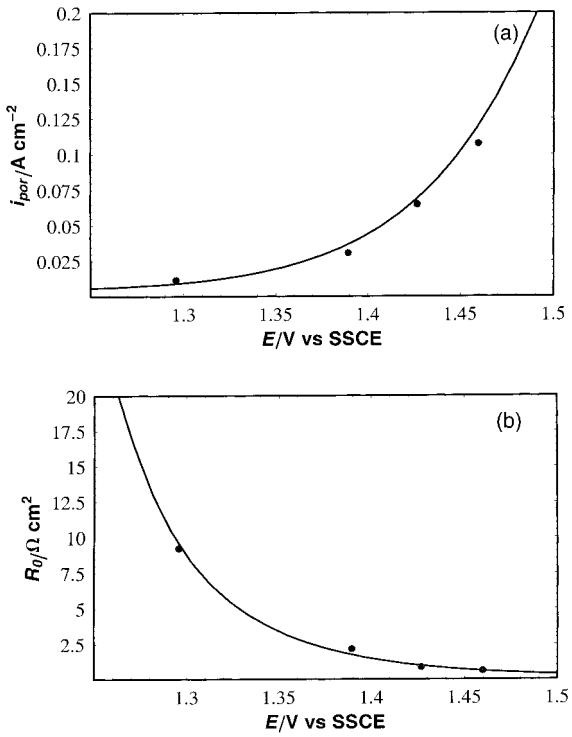

Fig. 5. Experimental values (•) for the steady-state current (a) and the zero frequency resistance (b) of the porous PbO_2 -electrode plotted together with the theoretical curve (solid line). With an external pressure of 3.6 kg cm^{-2} .

Table 1. Parameters used in the simulation of the polarization resistance, R_0, the steady-state current, i_f and the impedance of the porous electrode

	Nonpressurized electrode	Pressurized electrode
k_1°	3.5×10^{-13}	2.0×10^{-12}
k_2°	4.25×10^{-13}	8.5×10^{-13}
E_1°	1.26	1.20
E_2°	1.31	1.24
α_1	0.50	0.34
α_2	0.60	0.56
β_{max}	4.0×10^{-11}	1.0×10^{-10}

relaxation interferes with the charge transfer relaxation. The impedance spectra at these potentials correspond to the intermediate case with $\omega_1/\omega_0 > 1.58$, and the impedance can therefore be calculated by Equation 15. At more positive potentials, 1.42 and 1.45 V, the semicircle in the low frequency part of the spectra starts to merge into the linear part, as predicted by the model when the frequency of the reaction, ω_0, reaches the same level as the field diffusion frequency, ω_1.

Figures 6 show the experimental data for the electrodes made from 200 μm lead foil plotted together with data calculated from the model, while Figure 7 corresponds to experiments where an external pressure of 3.6 kg cm^{-2} is applied. Experimental and calculated data compare fairly well. The results show that the polarization resistance decreases with increasing positive potential, which indicates that the overall reaction is charge transfer controlled. The currents of the pressurized cells

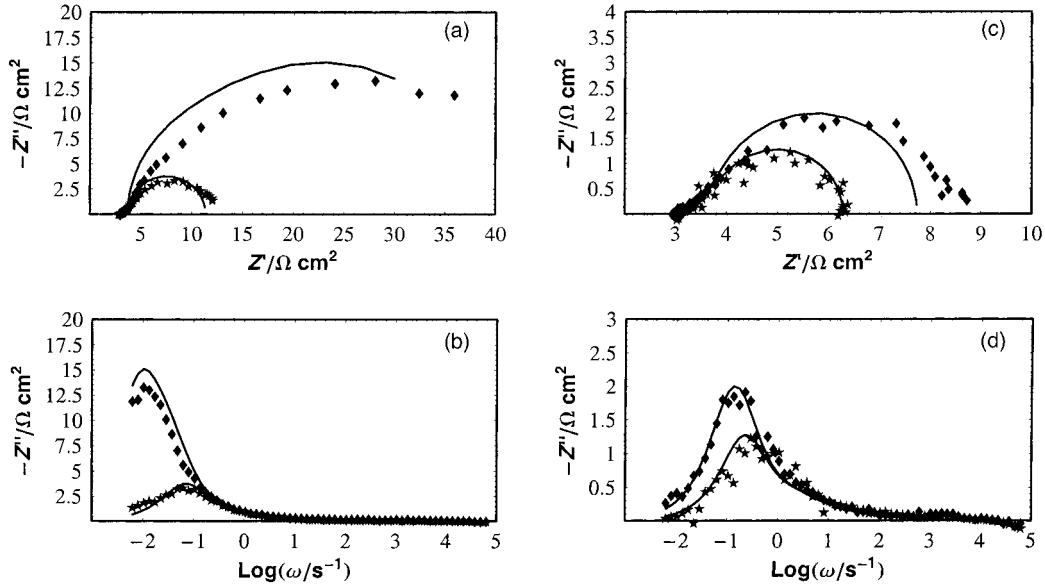

Fig. 6. Experimental and calculated impedance diagrams for a nonpressurized lead dioxide electrode. Nyquist plots: (a) ◆ 1.29 V and ★ 1.38 V, (b) ◆ 1.42 V and ★ 1.45 V. Imaginary part as a function of the frequency. (c) ◆ 1.29 V and ★ 1.38 V, (d) ◆ 1.42 V and ★ 1.45 V. Solid line corresponds the model calculations at the same potentials.

were considerably higher than for the nonpressurized cells, Figure 4, and was previously explained by the higher degree of interparticle contact in the pressurized cells [17]. A higher degree of interparticle contact is also evident from the low values of the ohmic resistance (as measured by the high frequency limit of the impedance spectra) for pressurized cells, Figure 7, compared to the nonpressurized ones, Figure 6. However, it was shown in an earlier paper [17] that the pore resistance did not increase in proportion to the thickness of the electrode as one might expect. This is probably due to a decrease in the effective resistance in the interior of the electrode as the formation time is increased. Nonelectrochemical measurements of the porosity showed that the relative pore volume increased with the thickness of the electrode causing the effective resistivity in the porous electrode to decrease [17].

Three parameters were evaluated from the experimental data, R_{por}, R_0 and ω_0, and used to calculate the pore volume, v_p, and the active surface area, S_c, Table 2. From the experimentally determined parameters, ω_1 can be calculated according to Equation 10. In addition, the three parameters R_{por}, R_0 and ω_0 are coupled to the physical parameters through two relations (Equations 7

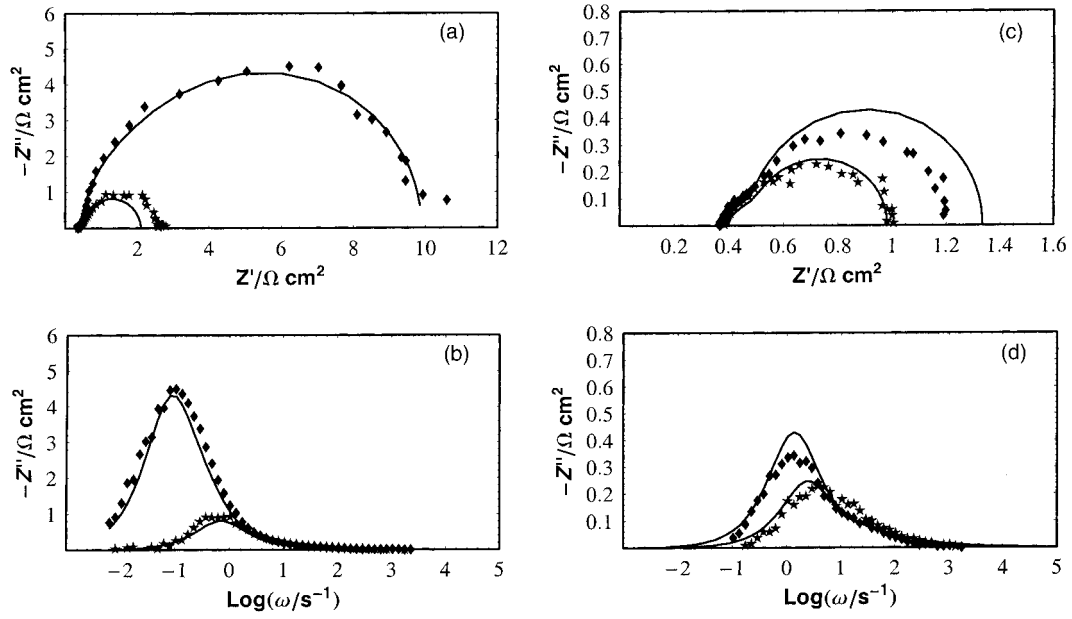

Fig. 7. Experimental and calculated impedance diagrams for a pressurized lead dioxide electrode. Nyquist plots: (a) ◆ 1.29 V and ★ 1.38 V, (b) ◆ 1.42 V and 1.45 V. Imaginary part as a function of the frequency. (c) ◆ 1.29 V and ★ 1.38 V, (d) ◆ 1.42 V and ★ 1.45 V. Solid line corresponds the model calculations at the same potentials.

and 12) with six quantities (C_{dl}, d, v_p, S_c, ρ_2^*, f). Thus, four of these have to be measured independently or by some good reason assumed. We have chosen to assign a value of $50\,\mu F\,cm^{-2}$ to the double layer capacity, C_{dl}, and 2 for the tortuosity factor [23], f. The bulk resistivity of the electrolyte, ρ_2^* can be calculated and for the sulphuric acid concentration used $\rho_2^* = 1.25\,\Omega\,cm$ [24]. The thickness of the electrode, d, is given as the thickness of the lead consumed in the formation process multiplied by a factor 2 for cells without external pressure and a factor of 1.5 for cells where pressure was applied (Pb has a Pilling–Bedworth ratio of 1.4). The remaining quantities (v_p, S_c,) were calculated from these parameters (C_{dl}, d, ρ_2^*, f) together with the parameters obtained experimentally (R_{por}, R_0 and ω_0). The reason for extracting v_p and S_c from the model was that a comparison with experimental data (obtained by independent measurements) was possible. The relative pore volume was estimated by water intrusion and the active surface area was obtained from BET measurements. The calculated values for the active surface area are in reasonable agreement with the experimental values. Table 2. However, the relative pore volume is underestimated in the model. This is probably due to a large number of macroscopic pores that contribute to the relative pore volume measured by water intrusion, but which do not function as pores in the electrochemical sense. This was further shown by looking at the cross section of the electrodes with SEM [17], which showed that, for the nonpressurized electrodes, considerable amounts of the particles were in bad contact with the rest of the electrode. For the pressurized electrode this effect was less pronounced.

Even though the absolute values of the calculated parameters are affected with some errors, impedance spectroscopy can be used in a diagnostic way to follow the health of the battery by measuring the change in the physical properties as a function of time and by using the impedance spectra for a fully charged battery as a reference.

In addition, the experimental steady-state current of the porous electrode was compared to the steady-state current predicted by the impedance model, by fitting the simulated impedance spectra to the experimental ones. The agreement between the experimental data and the calculated values of, not only the impedance data, but also the d.c.-current levels show that the a.c.-analysis in a thorough way can be extended to include the steady-state current for porous electrodes. For thick electrodes, or for electrodes under charge conditions, the experimental results show that the steady-state current has to be corrected for the porous nature of the electrode. By using the impedance model for porous electrodes this task is simplified considerably, Equation 20.

5. Conclusions

It is shown that an impedance model for porous macrohomogeneous electrodes can be used for Planté

Table 2. Parameters used in the analysis of the impedance data

	Assigned input values				Values obtained from the impedance model and experiments*		
	C_{dl}	ρ_2^*	d	f	S_c	v_p	R_{por}
Nonpressurized electrodes	$50\ 10^{-6}$	1.25	0.04	2	88.9	0.044	0.75
Pressurized electrodes	$50\ 10^{-6}$	1.25	0.03	2	57.0	0.19	0.135
Nonpressurized electrodes (Experimental)					50.6	0.19	0.75
Pressurized electrodes (Experimental)							0.135

	$\omega_0^\dagger$				R_0				i_{por}				$\omega_{1/}\omega_0$			
E	1.29	1.38	1.42	1.45	1.29	1.38	1.42	1.45	1.29	1.38	1.42	1.45	1.29	1.38	1.42	1.45
Nonpressurized electrodes (Simulation)	0.016	0.074	0.14	0.227	35.5	8.37	4.69	3.19	0.0025	0.0087	0.016	0.025	15.4	3.39	1.76	1.10
Pressurized electrodes (Simulation)	0.124	0.721	1.37	2.42	9.52	1.75	0.98	0.61	0.0089	0.037	0.068	0.119	24.1	4.16	2.18	1.23
Nonpressurized electrodes (Experimental)					32	8.51	5.15	3.11	0.0044	0.0069	0.0097	0.016				
Pressurized electrodes (Experimental)					9.24	2.15	0.84	0.60	0.011	0.031	0.065	0.107				

*S_c and v_p was calculated from the assigned parameters together with ω_1 obtained from Equation 10 and R_{por}
Expzerimental values of S_c and v_p were obtained from BET-measurements (S_c) and water intrusion (v_p)
R_{por} was obtained from the experimental impedance spectra at potentials where the high frequency end of the semicircle could be extrapolated to the real impedance axes. R_{por} given in the table is the mean value
† Calculated as $\omega_0 = 1/(R_p C_{dl})$

formed lead dioxide electrodes to give information about physical properties. The steady-state current for the porous electrode can be calculated from the impedance model and compared to experimentally determined values. Thus the d.c. and a.c. characteristics are linked and the total capacitance can be calculated. Three experimental parameters, R_{por}, R_0 and ω_0, were used in the modelling of the impedance spectra. From the theoretical model, clusters of parameters are obtained and in order to obtain detailed information on a particular property, for example, the active surface area, the pore volume or cell capacitance, additional information from independent measurements are needed.

Acknowledgements

This work received financial support from the Swedish National Board for Industrial and Technical Development (NUTEK).

References

1. F. Huet, *J. Power Sources* **70** (1998) 59.
2. V.V. Viswanathan, A.J. Salkind, J.J. Kelley and J.B. Ockerman, *J. Appl. Electrochem.* **25** (1995) 716.
3. V.V. Viswanathan, A.J. Salkind, J.J. Kelley and J.B. Ockerman, *J. Appl. Electrochem.* **25** (1995) 729.
4. R.T. Barton and P.J. Mitchell, *J. Power Sources* **27** (1989) 287.
5. M. Hughes, R.T. Barton, S.A.G.R. Karunathilaka and N.A. Hampson, *J. Appl. Electrochem.* **16** (1986) 555.
6. J. Jindra, M. Musilova, J. Mrha and A.A. Taganova, *J. Power Sources* **37** (1992) 403.
7. R. de Levie, *Electrochim. Acta* **8** (1963) 751.
8. R. de Levie, *Electrochim. Acta* **9** (1964) 1231.
9. K. Eloot, F. Debuyck, M. Moors and A.P. Vanpeteghem, *J. Appl. Electrochem.* **25** (1995) 326.
10. H. Keiser, K.D. Beccu and M.A. Gutjahr, *Electrochim. Acta* **21** (1976) 539.
11. M. Keddam, C. Rakotomawo and H. Takenouti, *J. Appl. Electrochem.* **14** (1984) 437.
12. G. Paasch, K. Micka and P. Gersdorf, *Electrochim. Acta* **38** (1993) 2653.
13. J.P. Candy, P. Fouilloux, M. Keddam and H. Takenouti, *Electrochim. Acta* **26** (1981) 1029.
14. J.P. Candy, P. Fouilloux, M. Keddam and H. Takenouti, *Electrochim. Acta* **27** (1982) 1585.
15. C. Cachet and R. Wiart, *Electrochim. Acta* **29** (1984) 145.
16. J. Newman, *J. Electrochem. Soc.* **142** (1995) 97.
17. I. Petersson, B. Berghult and E. Ahlberg, *J. Power Sources* **74** (1998) 68.
18. B.V. Tilak, S. Venkatesh and S.K. Rangarajan, *J. Electrochem. Soc.* **136** (1989) 1977.
19. I. Petersson, E. Ahlberg and B. Berghult, *J. Power Sources* **76** (1998) 98.
20. G. Bech-Nielsen, *Electrochim. Acta* **19** (1974) 821.
21. G. Bech-Nielsen, *Electrochim. Acta* **21** (1976) 627.
22. G. Bech-Nielsen, *Electrochim. Acta* **23** (1978) 425.
23. F.M. Delnick, D. Ingersoll and D. Firsich, *in* Third International Seminar on 'Double-Layer Capacitors and Similar Energy Storage Devices', Deerfield Beach, FL, 6–8 Dec. (1993).
24. H. Bode, 'Lead–Acid Batteries' (J. Wiley & Sons, New York, 1977).